Revised manuscript for publication in *ApJ*, January 24, 2022
Preprint typeset using LaTeX style emulateapj v. 5/2/11

arXiv:1207.0722v2 [astro-ph.EP] 13 Jul 2012

CHEMICAL TIMESCALES IN THE ATMOSPHERES OF HIGHLY ECCENTRIC EXOPLANETS

Channon Visscher
Department of Space Studies, Southwest Research Institute, Boulder, CO, 80302, USA
Revised manuscript for publication in ApJ*, January 24, 2022*

ABSTRACT

Close-in exoplanets with highly eccentric orbits are subject to large variations in incoming stellar flux between periapse and apoapse. These variations may lead to large swings in atmospheric temperature, which in turn may cause changes in the chemistry of the atmosphere from higher CO abundances at periapse to higher CH_4 abundances at apoapse. Here we examine chemical timescales for CO$\rightleftarrows$$CH_4$ interconversion compared to orbital timescales and vertical mixing timescales for the highly eccentric exoplanets HAT-P-2b and CoRoT-10b. As exoplanet atmospheres cool, the chemical timescales for CO$\rightleftarrows$$CH_4$ tend to exceed orbital and/or vertical mixing timescales, leading to quenching. The relative roles of orbit-induced thermal quenching and vertical quenching depend upon mixing timescales relative to orbital timescales. For both HAT-P-2b and CoRoT-10b, vertical quenching will determine disequilibrium CO$\rightleftarrows$$CH_4$ chemistry at faster vertical mixing rates ($K_{zz} > 10^7$ cm^2 s^{-1}), whereas orbit-induced thermal quenching may play a significant role at slower mixing rates ($K_{zz} < 10^7$ cm^2 s^{-1}). The general abundance and chemical timescale results – calculated as a function of pressure, temperature, and metallicity – can be applied for different atmospheric profiles in order to estimate the quench level and disequilibrium abundances of CO and CH_4 on hydrogen-dominated exoplanets. Observations of CO and CH_4 on highly eccentric exoplanets may yield important clues to the chemical and dynamical properties of their atmospheres.

Subject headings: planetary systems — planets and satellites: atmospheres — planets and satellites: composition — planets and satellites: individual (HAT-P-2b, CoRoT-10b)

1. INTRODUCTION

For planets with high eccentricity, the large variations in flux received from their host stars may yield substantial variations in atmospheric temperature and dynamical behavior during the course of an orbit (Langton & Laughlin 2008; Laughlin et al. 2009; Iro & Deming 2010; Cowan & Agol 2011; Kane & Gelino 2011; Rauscher & Menou 2012; Lewis et al. 2012). In some cases, orbit-induced temperature variations may be large enough to produce a significant shifts in the chemical behavior of the planet. For example, the swing between high atmospheric temperatures at periapse and lower atmospheric temperatures at apoapse may shift equilibrium chemistry predictions from relatively higher CO abundances at periapse (toward a CO-dominated atmosphere) to relatively higher CH_4 abundances at apoapse (toward a CH_4-dominated atmosphere).

Large changes in the abundances of CO and CH_4 are of particular interest because these compounds strongly influence the spectral properties of exoplanet atmospheres (e.g., Seager & Sasselov 2000; Burrows et al. 2005; Charbonneau et al. 2007, 2008; Fortney et al. 2007; Barman 2008; Swain et al. 2008, 2009a,b, 2010; Désert et al. 2009; Madhusudhan & Seager 2009, 2011; Madhusudhan et al. 2011; Stevenson et al. 2010; Tinetti et al. 2010a,b; Beaulieu et al. 2011; Knutson et al. 2011; Lee et al. 2012; Shabram et al. 2011; Waldmann et al. 2012). Phase-dependent variations in the planetary spectrum (e.g., Barman et al. 2005; Fortney et al. 2006; Knutson et al. 2007, 2012; Showman et al. 2008, 2009; Cowan & Agol 2011; Lewis et al. 2012) may therefore also reflect changes in chemical composition of highly eccentric transiting exoplanets (see Table 1), particularly at wavelengths sensitive to CO and CH_4 (e.g., Lewis et al. 2012)

However, the extent of temperature-dependent variations in carbon chemistry throughout the orbit – and whether equilibrium chemistry at a given altitude prevails over orbital timescales – also depends upon the rate of CO$\rightleftarrows$$CH_4$ interconversion relative to the time elapsed between periapse and apoapse. Thermochemical equilibrium can be maintained throughout the orbit only if chemical timescales are less than orbital timescales. To study this effect, Iro & Deming (2010) estimated the CO$\rightleftarrows$$CH_4$ interconversion timescale for HD 80606b and HD 17156b using the kinetics of Bézard et al. (2002) and found that orbital timescales are generally much shorter than chemical timescales – indicative of disequilibrium chemistry – at pressure levels where orbit-induced temperature variations are expected to be significant. This behavior will occur on objects which are expected to have relatively low atmospheric temperatures (and therefore sluggish reaction kinetics) near apoapse, leading to orbit-induced thermal quenching wherein an equilibrium composition achieved near periapse survives to become a disequilibrium composition at apoapse.

The observed properties of highly eccentric exoplanets are subject to numerous variables including thermochemical and photochemical reaction rates, convective transport, and horizontal dynamical and radiative timescales. Here, we focus specifically on the role of thermochemical quench chemistry in response to vertical transport and eccentricity-induced atmospheric temperature variations, as this behavior may strongly influence observable CO and CH_4 abundances (even if photolysis occurs at higher altitudes). For simplicity, the rele-

TABLE 1
Highly-Eccentric ($e > 0.3$) Transiting Exoplanets

Object	a(AU)	e	p(days)	p_s(days)	M_J	R_J
HD 80606b	0.447	0.934	111.44	1.7	3.9	1.03
HD 17156b	0.163	0.682	21.22	3.6	3.3	1.02
CoRoT-10b	0.105	0.530	13.24	4.3	2.8	0.97
HAT-P-2b	0.068	0.517	5.63	1.9	8.9	1.16
HAT-P-34b	0.068	0.440	5.45	2.4	3.4	1.20
HAT-P-17b	0.088	0.346	10.34	5.9	0.5	1.01
WASP-8b	0.080	0.310	8.16	5.1	2.1	1.04

Note. — Data from Wright et al. (2011). The pseudo-synchronous rotation period p_s was calculated using the expressions of Hut (1981) as presented in Iro & Deming (2010).

vant timescale for the temperature variation is taken to be $0.5p$ (where p is the orbital period), which describes the time elapsed between temperature swings at periapse and apoapse. We first calculate the abundances of CO and CH_4 and CO$\rightleftarrows$$CH_4$ chemical timescales as a function of pressure, temperature, and metallicity in a solar-composition gas, using updated kinetics for CO$\rightleftarrows$$CH_4$ interconversion (Visscher et al. 2010b; Moses et al. 2011; Visscher & Moses 2011). The results are then compared to orbital and mixing timescales and pressure-temperature profiles of individual objects to estimate the quench levels and abundances of CO and the CH_4 as disequilibrium species. The primary objective of this study is to discuss a convenient method for exploring thermal quenching processes in the CO$\rightleftarrows$$CH_4$ system in exoplanet atmospheres. Although we focus on CO-abundant HAT-P-2b and CH_4-abundant CoRoT-10b as specific examples, the abundance and timescale results presented here may in principle be applied to any H_2-dominated substellar object that is subject to orbit-induced temperature variations.

2. CHEMICAL MODEL

2.1. *Equilibrium Chemistry and Abundances*

We develop a gas-phase chemical model based upon the thermochemical equilibrium models of Fegley & Lodders (1994), Lodders & Fegley (2002), and Visscher et al. (2006, 2010a). As in Lodders & Fegley (2002), we examine H-C-N-O chemistry over a range of pressures, temperatures, and metallicities so that the model results may be applied to a variety of substellar objects. Solar-composition elemental abundances are taken from Lodders (2010), and we consider the removal of $\sim 21\%$ of oxygen into rock-forming elements (Lodders 2004; Visscher & Fegley 2005). Figure 1 shows the equilibrium mole fraction abundances of CO and CH_4 as a function of pressure and temperature in a solar-metallicity gas. Also shown is the CO=CH_4 equal abundance boundary ($X_{CO} = X_{CH_4} = 0.5X_{\Sigma C}$), approximated by

$$\log P \approx 5.05 - 5807.5/T + 0.5[\mathrm{Fe/H}], \quad (1)$$

for P in bars and T in kelvins. At pressures and temperatures where methane is the dominant C-bearing gas (higher P, lower T), the mole fraction abundances of CH_4 and CO are given by

$$X_{CH_4} \approx X^*_{\Sigma C} m, \quad (2)$$

$$X_{CO} \approx X^*_{CO}(P,T) m^2, \quad (3)$$

where $X^*_{\Sigma C}$ is the total carbon abundance in a solar-metallicity gas ($\sim 4.5 \times 10^{-4}$; Lodders 2010), $X^*_{CO}(P,T)$ is the solar-metallicity abundance of CO as a function of pressure and temperature as plotted in Figure 1a, and m is the metallicity factor defined by $\log m = [\mathrm{Fe/H}]$ (Lodders & Fegley 2002; Visscher et al. 2006).

At pressures and temperatures where carbon monoxide is the dominant C-bearing gas (lower P, higher T), the mole fraction abundances of CO and CH_4 are given by

$$X_{CO} \approx X^*_{\Sigma C} m, \quad (4)$$

$$X_{CH_4} \approx X^*_{CH_4}(P,T), \quad (5)$$

where $X^*_{CH_4}(P,T)$ is the mole fraction abundance of CH_4 as a function of pressure and temperature in a solar metallicity gas, as plotted in Figure 1b. Unlike CO, which shows a strong (m^2) dependence on metallicity inside the CH_4 field, the methane abundance inside the CO field is independent of metallicity because it is proportional to the total carbon abundance (ΣC) but inversely proportional to the total oxygen abundance (ΣO). Note that these simple abundance approximations begin to break down at higher metallicities ($m > 30$) as heavy elements become significantly abundant relative to hydrogen and helium. For high-metallicity cases, mole fraction values can be calculated from solar elemental abundance ratios (Lodders 2010) with different values of m. A more complete description of the equilibrium chemical behavior of CO, CH_4, and other carbon-bearing species as a function of P, T, and m in substellar atmospheres can be found in Lodders & Fegley (2002).

2.2. *Chemical Kinetics and Timescales*

For CO-CH_4 quench kinetics we adopt the reaction scheme of Moses et al. (2011) and Visscher & Moses (2011), who identify two plausible mechanisms for CO$\rightleftarrows$$CH_4$ interconversion in substellar atmospheres. In general, the rate-limiting step for breaking/forming the C–O bond is

$$CH_3OH + M \rightleftarrows CH_3 + OH + M, \quad (6)$$

when CH_4 is the dominant C-bearing gas, and

$$CH_2OH + H \rightleftarrows CH_3 + OH, \quad (7)$$

when CO is the dominant C-bearing gas. However, the contribution of either pathway is significant enough that both should be considered when estimating the CO$\rightleftarrows$$CH_4$ interconversion rate in substellar atmospheres. The chemical timescale for CO$\rightarrow$$CH_4$ is thus given by

$$\tau_{\mathrm{chem}}(CO) = \frac{[CO]}{k_{6f}[CH_3OH][M] + k_{7f}[CH_2OH][H]}, \quad (8)$$

where k_{6f} and k_{7f} are the forward reaction rate constants for reactions (6) and (7), respectively. The chemical timescale for $CH_4$$\rightarrow$CO is given by

$$\tau_{\mathrm{chem}}(CH_4) = \frac{[CH_4]}{k_{6r}[CH_3][OH][M] + k_{7r}[CH_3][OH]}, \quad (9)$$

where k_{6r} and k_{7r} are the reverse reaction rate constants for reactions (6) and (7), respectively, taken from Jasper et al. (2007) and reversed to give k_{6f} and k_{7f} using the method described in Visscher & Moses (2011).

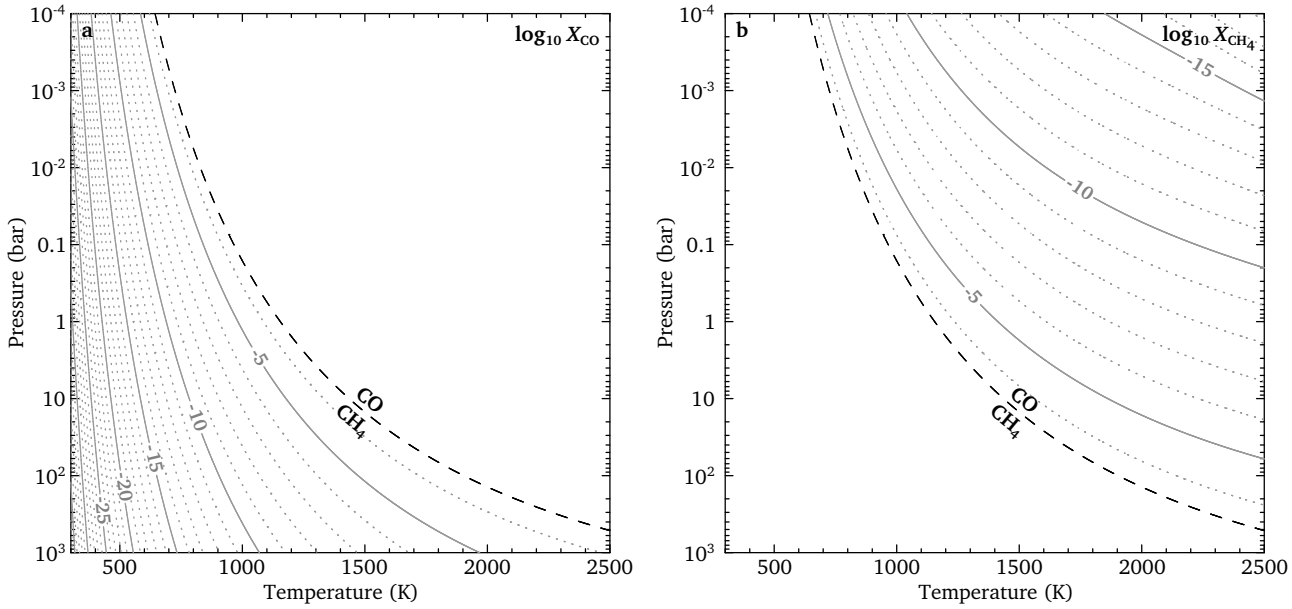


FIG. 1.— Equilibrium mole fraction abundance contours (on a logarithmic scale) for (a) CO and (b) CH_4 in a solar-composition gas at pressures and temperatures relevant for extrasolar giant planet atmospheres. In each panel, the dashed line denotes the CO = CH_4 equal-abundance boundary where $X_{CO} = X_{CH_4} \approx 0.5X_{\Sigma C}$. Figure after Lodders & Fegley (2002)

Using equilibrium abundances for OH, CO, CH_3, CH_4, CH_2OH and CH_3OH, the chemical timescales for $CH_4 \rightarrow CO$ and $CO \rightarrow CH_4$ are shown in Figure 2 (as contours on a logarithmic scale) as a function of pressure and temperature in a solar-metallicity gas. We also calculated chemical timescales at metallicities between [Fe/H] = −2 and [Fe/H] = +2. Over this range, the timescale for CO destruction, $\tau_{\rm chem}(CO)$, is independent of metallicity, whereas the timescale for CH_4 destruction as a function of metallicity is given by

$$\tau_{\rm chem}(CH_4) \approx \tau^*_{\rm chem}(CH_4)(P,T)m^{-1}, \qquad (10)$$

where $\tau^*_{\rm chem}(CH_4)(P,T)$ is the chemical timescale for $CH_4 \rightarrow CO$ as a function of pressure and temperature in a solar metallicity gas (plotted in Figure 2b) and m is the metallicity factor. Equation (10) demonstrates that higher metallicities result in shorter timescales (i.e., faster reaction kinetics) for $CH_4 \rightarrow CO$ chemistry over the range of pressures and temperatures considered here.

3. RESULTS AND DISCUSSION

The abundances in Figure 1 and the chemical timescales in Figure 2 can be compared with orbital and dynamical timescales as well as atmospheric pressure-temperature profiles for individual objects in order to estimate the quench level and abundances of disequilibrium species. Using CO-dominated HAT-P-2b and CH_4-dominated CoRoT-10b as specific examples, here we examine various profile/timescale intersections in order to explore $CO \rightleftarrows CH_4$ quench processes in exoplanet atmospheres, as these intersections represent some quench level with respect to orbital timescales. The guiding principle throughout the following discussion is that the chemical behavior in the $CO \rightleftarrows CH_4$ system is governed by the shortest available timescale in the system.

The planet-wide average temperature profiles at periapse and apoapse overlaid on the timescale and abundance plots are shown in Figure 3 for HAT-P-2b and Figure 4 for CoRoT-10b. The pressure-temperature profiles for HAT-P-2b are planetary average profiles derived from the general circulation models (GCMs) of Lewis et al. (2010, 2012). The CoRoT-10b profiles are from the one-dimensional models of Fortney et al. (2006, 2008, 2010) where the incident stellar radiation is assumed to be redistributed over the entire planet.

Because we are primarily interested in the temperature difference between periapse and apoapse (and its effect on thermochemistry), we focus on the time elapsed between these extremes irrespective of radiative timescales. However, orbit-induced temperature variations will exist only if the radiative timescale is less than the orbital period (e.g., see Cowan & Agol 2011, and references therein). Orbital timescales for the highly eccentric exoplanets listed in Table 1 are on the order of days, whereas radiative timescales at photospheric altitudes on such planets are typically on the order of hours (e.g., Laughlin et al. 2009; Iro & Deming 2010; Lewis et al. 2012). We thus adopt $0.5p$ (where p is the orbital period) as the characteristic orbital timescale throughout the following discussion, and time elapsed between periapse and apoapse is denoted in Figures 3 and 4 by the lines labeled $0.5p$. The time elapsed between noon and midnight is denoted by $0.5p_s$, which is one half of the pseudo-synchronous rotation period derived from Hut (1981) as presented in Iro & Deming (2010). Although we focus on orbital temperature variations in the present study, in principle diurnal variations in atmospheric chemistry could be explored using a similar approach, depending upon the relative dynamical and radiative timescales.

3.1. *Transport-induced Quenching*

In addition to orbit-induced temperature variations, atmospheric constituents will also be subject to convective vertical mixing. The mixing timescale ($\tau_{\rm mix}$) is esti-

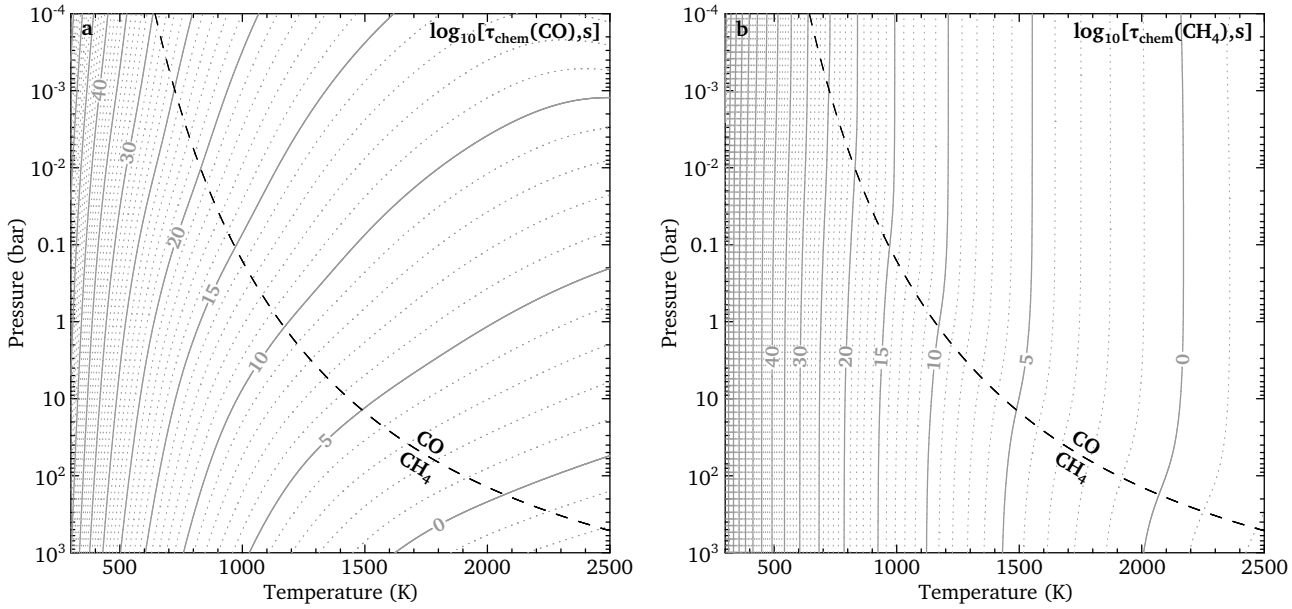


FIG. 2.— Chemical timescales (in seconds, on a logarithmic scale) for (a) the conversion of CO to CH_4 and (b) the conversion of CH_4 to CO in a solar-metallicity gas. The dashed line denotes the position of the CO = CH_4 equal abundance boundary. Figure after Lodders & Fegley (2002). See text for details.

mated using the expression

$$\tau_{\rm mix} = L^2/K_{zz}, \tag{11}$$

where L is the mixing length and K_{zz} is the eddy diffusion coefficient (Stone 1976; Smith 1998). Because the vertical mixing rate in extrasolar giant planets is unknown, K_{zz} is treated as a free parameter in the models. For hot giant planet atmospheres, it is reasonable to assume $L \sim 0.5H$ (Visscher & Moses 2011; Smith 1998) where H is the atmospheric scale height ($H = RT/\mu g$). If required, better estimates of L/H may be calculated on a case-by-case basis using the method of Smith (1998). The gravity is calculated from the mass and radius of the planet (see Table 1) and we assume a mean molecular mass of $\mu \sim 2.4$ g mole^{-1} for an H_2-dominated, solar-composition atmosphere.

The vertical quench level is defined as the altitude at which $\tau_{\rm mix} = \tau_{\rm chem}$ (Prinn & Barshay 1977; Fegley & Prinn 1985). The pressures and temperatures for which this condition occurs on each planet are shown in Figures 3 and 4 as filled circles with labeled solid lines denoting the estimated K_{zz} value (in cm^2 s^{-1}) for each case. The intersections of the atmospheric pressure-temperature profiles with the $\tau_{\rm mix} = \tau_{\rm chem}$ curves in Figures 3 and 4 indicate the location of transport-induced quench level (P_q, T_q) for different assumptions about the vertical mixing rate (characterized by K_{zz}). The quench level represents the lowest pressure (i.e., highest altitude) along the atmospheric profile for which equilibrium can be achieved in the presence of convective vertical mixing; at all pressures $< P_q$, the abundance of CO (for CO destruction) or CH_4 (for CH_4 destruction) will remain fixed at the equilibrium abundance achieved at P_q, T_q. As expected, high K_{zz} values result in quenching deep in the atmosphere whereas low K_{zz} values give quenching at lower atmospheric pressures. However, as discussed below, vertical mixing can only play a significant role in the atmospheres of highly eccentric exoplanets over orbital timescales if mixing timescales ($\tau_{\rm mix}$) are shorter than the time elapsed between periapse and apoapse ($0.5p$).

Cooper & Showman (2006) demonstrated that disequilibrium abundances of CO and CH_4 in the upper (observable) atmospheres of hot Jupiters are controlled by vertical quenching, and that horizontal transport may homogenize these abundances with longitude. In the present study we therefore do not examine the effects of horizontal transport, and focus instead on the relative roles of vertical quenching caused by convective mixing and thermal quenching caused by orbit-induced temperature variations. However, we note that strong horizontal winds may serve to homogenize disequilibrium abundances from either quenching mechanism (vertical or orbit-induced) in the upper atmospheres of highly eccentric exoplanets.

3.2. *Methane Quenching on HAT-P-2b*

On HAT-P-2b, CO is the dominant carbon-bearing gas and so we consider CH_4 quench chemistry. As the planet cools between periapse and apoapse, the equilibrium CH_4 abundance is predicted to greatly increase (e.g., see Figure 3c). However, equilibrium can only be maintained if CO→CH_4 conversion kinetics are fast enough to produce CH_4 over orbital timescales ($\tau_{\rm chem} \leq 0.5p$). We therefore examine CO→CH_4 chemical timescales (left hand panels in Figure 3) in order to determine whether the higher CH_4 abundances predicted by equilibrium can be produced as the atmosphere shifts from high temperatures at periapse to low temperatures at apoapse.

At relatively high pressures and temperatures, deep in the atmosphere, equilibrium can be maintained throughout the entire orbit if chemical timescales are always shorter than orbital timescales ($\tau_{\rm chem} < 0.5p$). For highly eccentric exoplanets, the lowest pressure for which this condition holds is given by the intersection of the apoapse profile and the orbital timescale ($0.5p$). On HAT-P-2b, the apoapse/$0.5p$ intersection occurs near the

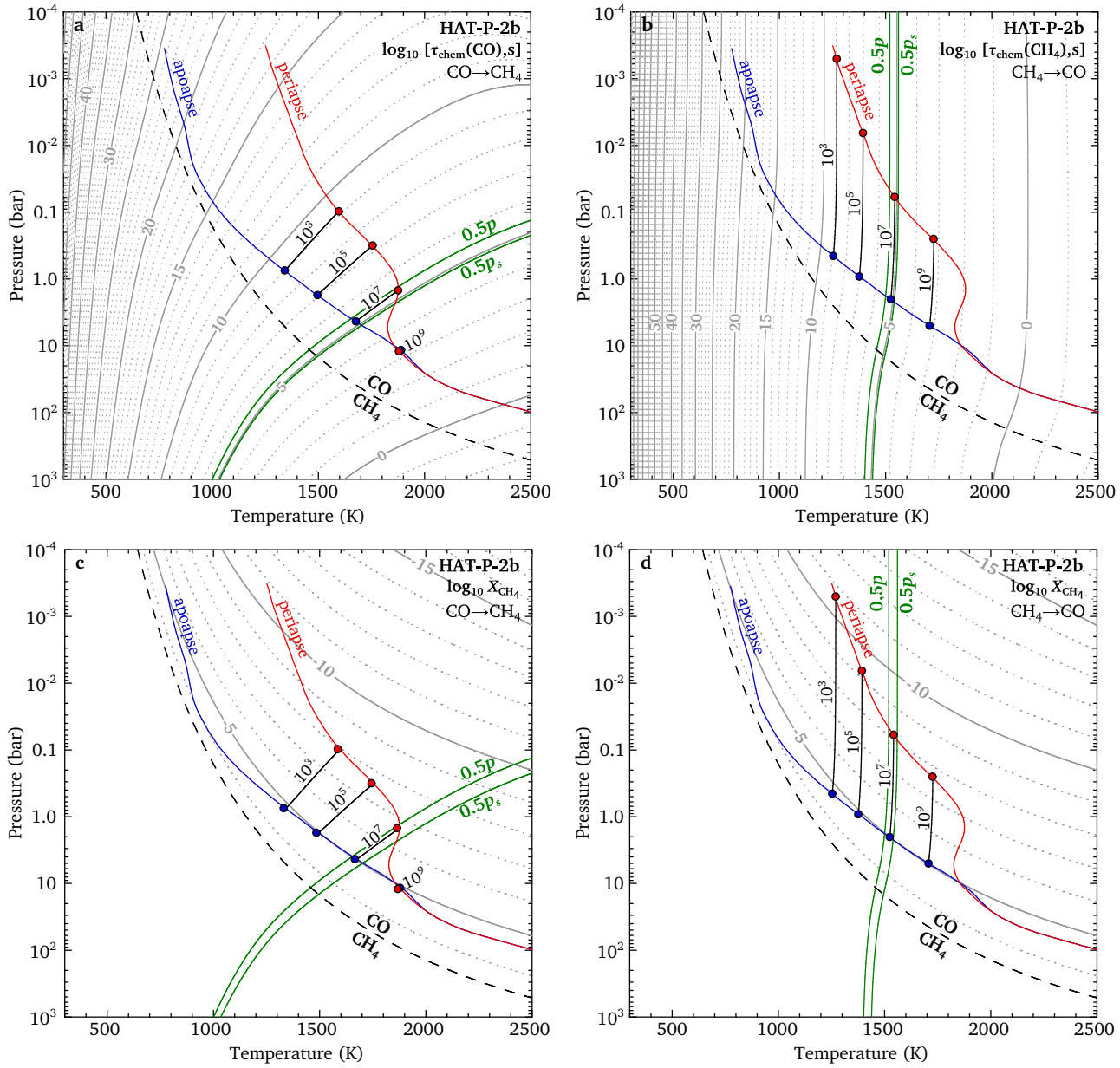


FIG. 3.— Chemical timescales (top panels; contours in seconds on a logarithmic scale) and equilibrium CH_4 abundances (bottom panels; mole fraction contours on a logarithmic scale) for CO→CH_4 conversion timescales (left panels) and CH_4→CO conversion timescales (right panels) on HAT-P-2b. Planet-wide average temperature profiles for HAT-P-2b are shown for apoapse (blue lines) and periapse (red lines). The solid green lines denote the time elapsed between periapse and apoapse ($0.5p$, where p is the orbital period) and the time elapsed between noon and midnight ($0.5p_s$, where p_s is the pseudo-synchronous rotation rate). The filled symbols with tie lines show where $\tau_{\rm mix} = \tau_{\rm chem}$ (i.e., the vertical quench level) for different values of K_{zz} (cm^2 s^{-1}) using the mixing length approach of Smith (1998) as presented in Visscher & Moses (2011). (A color version of this figure is available in the online journal.)

4-bar level (see Figure 3a), demonstrating that CO→CH_4 equilibrium chemistry – and the corresponding increase in the equilibrium abundance of CH_4 – can be maintained throughout the entire orbit only for $P \gtrsim 4$ bars. In the absence of vertical mixing, the equilibrium CH_4 mole fraction abundance at the $\sim$ 4-bar level can track eccentricity-induced temperature variations over orbital timescales by shifting from $\sim$ 1 ppm at periapse to $\sim$ 10 ppm near apoapse (see Figure 3c).

At lower pressures, however, orbit-induced temperature variations will quench CO→CH_4 conversion once $\tau_{\rm chem} > 0.5p$ as the planet moves between periapse and apoapse. Equilibrium compositions achieved during part of the orbit when the atmosphere is warmer ($\tau_{\rm chem} < 0.5p$) will quench once $\tau_{\rm chem} > 0.5p$ as the atmosphere cools. This boundary is represented by the $0.5p$ curve between the apoapse and periapse profiles in Figure 3a. Quenched CH_4 abundances resulting from orbit-induced thermal quenching can likewise be estimated by the position of the orbital timescale ($0.5p$) curve in Figure 3c. Note that the portion of the orbit over which equilibrium is achieved (i.e., $\tau_{\rm chem} < 0.5p$) decreases with altitude in the upper atmosphere of HAT-P-2b.

The intersection between the periapse profile and the

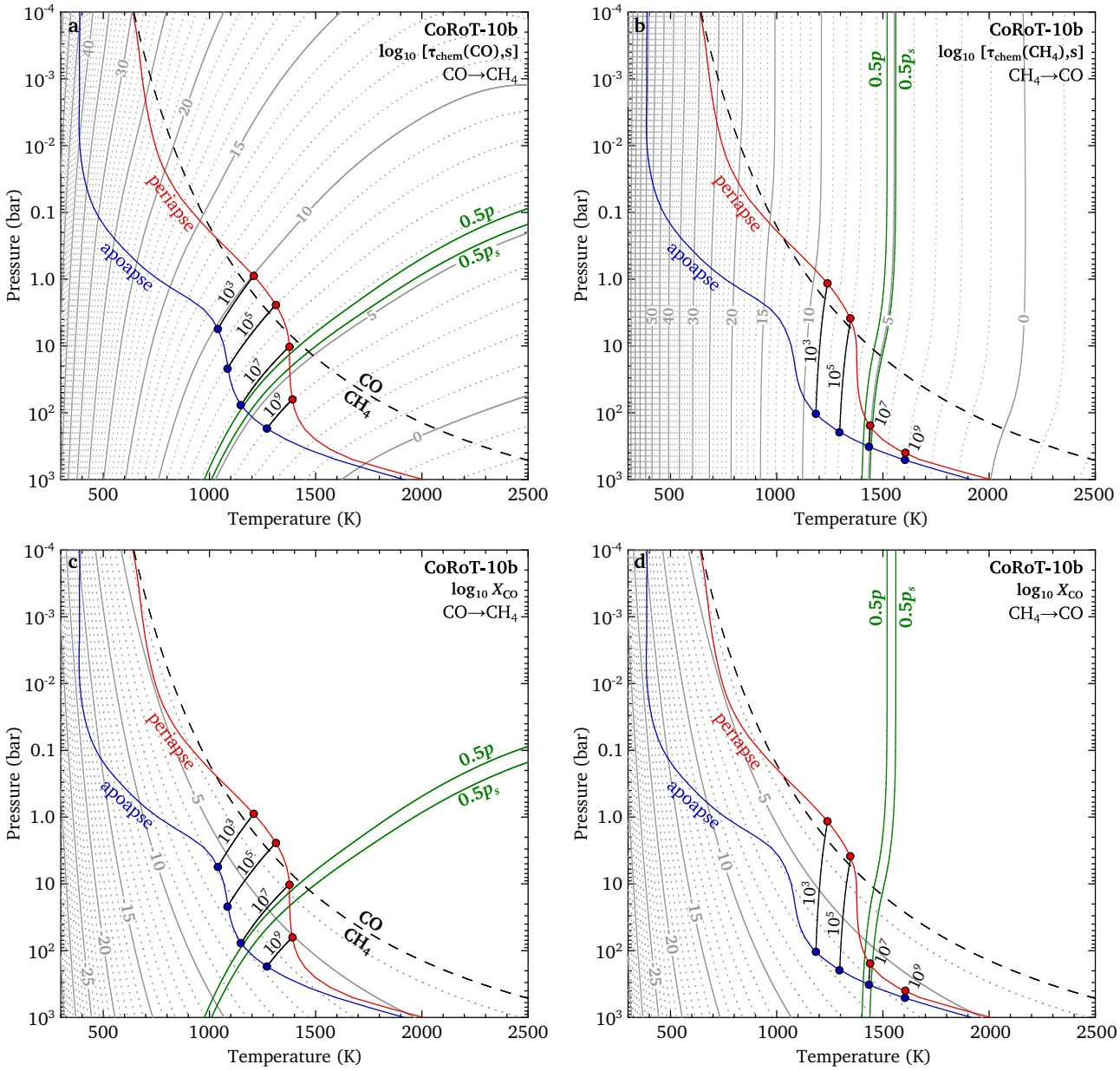


FIG. 4.— Chemical timescales (top panels; contours in seconds on a logarithmic scale) and equilibrium CO abundances (bottom panels; mole fraction contours on a logarithmic scale) for CO→CH_4 conversion timescales (left panels) and CH_4→CO conversion timescales (right panels) on CoRoT-10b. Planet-wide average temperature profiles for CoRoT-10b are shown for apoapse (blue lines) and periapse (red lines). The solid green lines denote the time elapsed between periapse and apoapse ($0.5p$) and the time elapsed between noon and midnight ($0.5p_s$). The filled symbols with tie lines show where $\tau_{\rm mix} = \tau_{\rm chem}$ (i.e., the vertical quench level) for different values of K_{zz} (cm^2 s^{-1}). (A color version of this figure is available in the online journal.)

$0.5p$ curve represents the highest altitude (i.e., lowest P) in the atmosphere at which equilibrium can be achieved at any point during the orbit, with respect to orbital timescales. In Figure 3a, the intersection between periapse and the $0.5p$ curve occurs near the 1-bar level. At this intersection, CO→CH_4 proceeds over orbital timescales because $\tau_{\rm chem}({\rm CO}) = 0.5p$. As temperatures cool from periapse to apoapse (moving left horizontally from the periapse/$0.5p$ intersection in Figure 3a), the rate of CO destruction (and hence CH_4 production) decreases and quenches when $\tau_{\rm chem}({\rm CO}) > 0.5p$. For HAT-P-2B, this suggests orbit-induced thermal quenching of ~ 0.1 ppm CH_4 at the $\sim$ 1-bar level throughout the orbit, far below the equilibrium abundance of $\sim$ 10 ppm predicted at apoapse temperatures (see Figure 3c).

However, this thermal quenching scenario neglects the role of vertical transport. The relative importance of vertical versus orbit-induced thermal quenching depends upon the transport timescale relative to the orbital timescale. As can be seen in Figure 3, the orbital timescale for HAT-P-2b is roughly equivalent to a mixing timescales characterized by $K_{zz} \sim 10^7$ cm^2 s^{-1}. For $K_{zz} < 10^7$ cm^2 s^{-1}, orbit-induced thermal quenching from periapse to apoapse will likely determine the CH_4 abundance because vertical mixing timescales exceed the time elapsed between periapse and apoapse

($\tau_{\rm mix} > 0.5p$). Thermal quenching in this scenario is expected to yield very low ($0.01-1$ ppm) CH_4 abundances in the upper atmosphere throughout the orbit.

If we assume faster vertical mixing rates, vertical quenching will dominate because $\tau_{\rm chem} < 0.5p$. For $K_{zz} > 10^7$ cm^2 s^{-1}, transport-induced quenching will give ~ 10 ppm CH_4 throughout the upper atmosphere of HAT-P-2b at apoapse (see Figure 3c), because thermally-quenched CH_4 will be overwhelmed by much larger quantities of CH_4 transported from higher pressures along the apoapse profile. As noted by Lewis et al. (2012), even higher CH_4 abundances may be possible if HAT-P-2b has a reduced metallicity and/or an enhanced C/O ratio (e.g., see Moses et al. 2012). Estimates of the quenched CH_4 abundance and the expected quench mechanism are summarized in Table 2. The large difference in predicted abundances as a function of K_{zz} suggest that observations of the CH_4 abundance on highly eccentric exoplanets may yield information about atmospheric mixing rates.

3.3. *Carbon Monoxide Quenching on CoRoT-10b*

On the cooler CoRoT-10b, CH_4 is the dominant C-bearing gas and so we consider CO quench chemistry. Unlike CH_4 chemistry on HAT-P-2b, the equilibrium CO abundance on CoRoT-10B is expected to *decrease* as the planet moves from periapse to apoapse (see Figure 4c), leading to quenching of excess CO. We thus first consider CO→CH_4 kinetic timescales as the planet nears apoapse. The intersection of the apoapse profile and orbital timescale ($0.5p$) occurs near the 90-bar level in Figure 4c, indicating that CO→CH_4 equilibrium chemistry can be maintained throughout the orbit if $P \gtrsim 90$ bars.

As the planet swings back toward periapse, the equilibrium abundance of CO is predicted to rapidly increase with increasing temperatures. However, CO can only be produced if CH_4→CO kinetics (Figure 4b) are sufficiently fast relative to orbital timescales. We must therefore examine CH_4→CO chemical timescales to determine the highest altitude (lowest P) at which equilibrium can be maintained throughout the orbit. The intersection between the apoapse profile and the $0.5p$ curve for CH_4→CO timescales occurs near the 300-bar level on CoRoT-10b: i.e., only for atmospheric pressures greater than ~ 300 bars can CO⇄CH_4 equilibrium chemistry be maintained over orbital timescales, shifting from ~ 0.3 ppm CO at apoapse to ~ 3 ppm CO at periapse (see Figure 4d). However, note that CO abundances in the upper atmosphere of CoRoT-10b at apoapse will more likely be determined by orbit-induced thermal quenching or vertical quenching, depending upon the rate of vertical mixing in its atmosphere.

The intersection between periapse and the $0.5p$ curve represents the lowest pressure level at which equilibrium can be achieved at any point during the orbit with respect to orbital timescales. For CoRoT-10b, the intersection between the periapse profile and the $0.5p$ curve occurs near 14 bars for CO→CH_4 chemistry (Figure 4a). At pressure levels between the apoapse/$0.5p$ intersection (~ 90 bars) and the periapse/$0.5p$ intersection (~ 14 bars), CO→CH_4 conversion is quenched whenever $\tau_{\rm chem} > 0.5p$ (this boundary is represented by the $0.5p$ curve between the apoapse and periapse profiles in Figure 4b). From a comparison of orbital timescales ($0.5p$ curve) and CO abundances in Figure 4c, we thus might expect thermally-quenched CO abundances of $\sim 0.1-100$ ppm above the ~ 90-bar pressure level on CoRoT-10b.

TABLE 2
Estimated Quench Abundances at $P < 1$ bar

K_{zz} (cm^2 s^{-1})	HAT-P-2b CH_4	CoRoT-10b CO
10^3	0.01-0.1 ppm (t)	$\geq$100 ppm (t)
10^5	0.03-0.1 ppm (t)	$\geq$100 ppm (t)
10^7	10 ppm (v)	100 ppm (v, t)
10^9	10 ppm (v)	10 ppm (v, t)

Note. — The notations (v) and (t) denote whether the quenching mechanism is predominantly caused by vertical mixing or by orbit-induced thermal variations, respectively.

For example, orbit-induced thermal quenching at the $\sim$ 14-bar level (the periapse/$0.5p$ intersection) would yield ~ 100 ppm CO throughout the orbit, in excess of the equilibrium abundance of ~ 1 ppm CO predicted at apoapse. This will also overwhelm the $\sim 0.1-1$ ppm CO predicted from vertical quenching over a range of K_{zz} values ($10^3 - 10^7$ cm^2 s^{-1}). Once present at lower pressure levels, CO cannot readily be converted back into CH_4 because $\tau_{\rm chem}({\rm CO}) > 0.5p$ (i.e., it is quenched) and $\tau_{\rm chem}({\rm CO}) > \tau_{\rm chem}(CH_4)$ (i.e., the CO production rate exceeds the CO destruction rate). Although CO production via CH_4→CO is also quenched at these altitudes, high abundances of CO are maintained because there is no way to destroy it thermochemically. In addition, as noted above, rapid horizontal transport would tend to homogenize this disequilibrium abundance (e.g., Cooper & Showman 2006). For slower mixing rates ($K_{zz} < 10^7$ cm^2 s^{-1}) it thus appears plausible that thermal quenching from eccentricity-induced temperature variations determines the CO abundance in the upper atmosphere of CoRoT-10b.

As for HAT-P-2b, the orbital timescale for CoRoT-10b is roughly equal to vertical mixing timescales characterized by $K_{zz} \sim 10^7$cm^2 s^{-1}, and we therefore expect vertical mixing to play a role for $K_{zz} \gtrsim 10^7$ cm^2 s^{-1}. Note that for these cases, vertical quenching along the periapse profile may determine a CO abundance which subsequently undergoes thermal quenching at lower pressures. For example, quenching at $K_{zz} \sim 10^7$ or $\sim 10^9$ cm^2 s^{-1} at periapse would yield quenched CO abundances of ~ 100 or ~ 10 ppm, respectively, throughout much of the upper atmosphere. These quantities of CO would prevail via orbit-induced thermal quenching as the planet moves from periapse to apoapse and overwhelm disequilibrium CO abundances that result from vertical quenching ($\tau_{\rm chem} = \tau_{\rm mix}$) along the apoapse profile.

Estimates of the upper atmospheric ($P < 1$ bar) quenched CO abundance and the expected quench mechanism(s) are summarized in Table 2. Although the results for CoRoT-10b do not show large differences in abundance as a function as K_{zz}, they consistently predict disequilibrium CO abundances 2-4 orders of magnitude in excess of equilibrium abundances predicted at apoapse.

3.4. *Nitrogen Quench Chemistry*

Other chemical systems may also respond to eccentricity-induced temperature variations. For example, large changes in atmospheric temperature may shift equilibrium chemistry predictions from relatively higher N_2 abundances at periapse to relatively higher NH_3 abundances at apoapse. To explore this effect, we calculated chemical timescales for $N_2 \rightleftarrows NH_3$ interconversion using the updated reaction mechanism described in Moses et al. (2011). For highly eccentric exoplanets, the quench process of most interest is $N_2 \rightarrow NH_3$ as the planet swings from periapse to apoapose (where higher NH_3 abundances are predicted). However, compared to the $CO \rightleftarrows CH_4$ system, $N_2 \rightleftarrows NH_3$ interconversion generally quenches at higher pressures, deeper in the atmosphere, where orbit-induced temperature variations are smaller. We thus expect orbit-induced thermal quenching to play a relatively minor role on HAT-P-2b and CoRoT-10b, yielding variations in the NH_3 abundance of less than an order of magnitude. Vertical quenching will more likely determine the abundance of NH_3 in the upper atmospheres of these highly eccentric exoplanets.

4. SUMMARY AND CONCLUSIONS

Equilibrium abundances for CO and CH_4 and chemical timescales for $CO \rightleftarrows CH_4$ interconversion were calculated as a function of pressure, temperature, and metallicity. A comparison of the abundance and timescale plots with atmospheric pressure-temperature profiles can be used to estimate the quench levels and abundances of CO and CH_4 for a variety of substellar objects. In principle, this approach can be applied for any substellar object with an H_2-dominated atmosphere that is subject to eccentricity-induced temperature variations. Overall, orbit-induced thermal quenching tends to favor CO over CH_4 because CO is the higher-temperature species and because chemical reactions proceed more rapidly at periapse than at apoapse. Moreover, equilibrium can be maintained to higher altitudes on warmer CO-dominated objects than on cooler CH_4-dominated objects, with respect to orbital and vertical mixing timescales.

Whether vertical quenching or orbit-induced thermal quenching governs disequilibrium $CO \rightleftarrows CH_4$ chemistry depends upon the orbital timescale relative to the mixing timescale (as a function of K_{zz}) along the atmospheric profile. In some cases, vertical quenching along the periapse profile may govern the disequilibrium abundances of CH_4 and CO throughout the upper atmosphere over the entire orbit. For both HAT-P-2b and CoRoT-10b, the effect of orbit-induced thermal quenching is roughly equivalent to transport-induced quenching assuming $K_{zz} \sim 10^7$ cm^2 s^{-1}. For lower K_{zz} values ($< 10^7$ cm^2 s^{-1}), thermal quenching may have a significant effect, whereas quenching via vertical transport will determine disequilibrium abundances of CO and CH_4 at higher K_{zz} values ($> 10^7$ cm^2 s^{-1}). For $CO \rightleftarrows CH_4$ chemistry, differences in the quenching mechanism may result in large differences in the abundances of disequilibrium carbon-bearing species. Refinements to atmospheric structure models and improved observational estimates of CO and CH_4 on highly eccentric exoplanets may yield important clues to the chemical and dynamical behavior of their atmospheres. Further development of the chemical models, including the consideration of photochemical production and loss rates throughout the orbit, may likewise provide improved abundance estimates of disequilibrium species throughout the upper atmospheres of highly eccentric transiting exoplanets.

Thanks to J. Moses and the anonymous referee for helpful comments on the manuscript, to J. Moses and N. Lewis for interesting discussions about orbital variations and quench chemistry, and to N. Lewis and J. Fortney for providing atmospheric profiles. This research was supported by the NASA Planetary Atmospheres Program (NNX10AF64G) and has made use of the Exoplanet Orbit Database and the Exoplanet Data Explorer at exoplanets.org.

REFERENCES

Barman, T. S. 2008, ApJ, 676, L61
Barman, T. S., Hauschildt, P. H., & Allard, F. 2005, ApJ, 632, 1132
Beaulieu, J.-P., Tinetti, G., Kipping, D.M., et al. 2011, ApJ, 731, 16
Bézard, B., Lellouch, E., Strobel, D., Maillard, J.-P., & Drossart, P. 2002, Icarus, 159, 95
Burrows, A., Hubeny, I., & Sudarsky, D. 2005, ApJ, 625, L135
Charbonneau, D., Brown, T. M., Burrows, A., & Laughlin, G. 2007, in Protostars and Planets V, ed. B. Reipurth, D. Jewitt, & K. Keil (Tuscon, AZ: Univ. Arizona Press), 701–716
Charbonneau, D., Knutson, H. A., Barman, T., et al. 2008, ApJ, 686, 1341
Cooper, C. S., & Showman, A. P. 2006, ApJ, 649, 1048
Cowan, N. B., & Agol, E. 2011, ApJ, 726, 82
Désert, J., Lecavelier des Etangs, A., Hébrard, G., et al. 2009, ApJ, 699, 478
Fegley, B., Jr., & Lodders, K. 1994, Icarus, 110, 117
Fegley, B., Jr., & Prinn, R. G. 1985, ApJ, 299, 1067
Fortney, J. J., Cooper, C. S., Showman, A. P., Marley, M. S., & Freedman, R. S. 2006, ApJ, 652, 746
Fortney, J. J., Lodders, K., Marley, M. S., & Freedman, R. S. 2008, ApJ, 678, 1419
Fortney, J. J., Marley, M. S., & Barnes, J. W. 2007, ApJ, 659, 1661
Fortney, J. J., Shabram, M., Showman, A. P., et al. 2010, ApJ, 709, 1396
Hut, P. 1981, A&A, 99, 126
Iro, N., & Deming, L. D. 2010, ApJ, 712, 218
Jasper, A., Klippenstein, S., Harding, L., & Ruscic, B. 2007, J. Phys. Chem. A, 111, 3932
Kane, S. R., & Gelino, D. M. 2011, ApJ, 741, 52
Knutson, H. A., Charbonneau, D., Allen, L. E., et al. 2007, Nature, 447, 183
Knutson, H. A., Madhusudhan, N., Cowan, N. B., et al. 2011, ApJ, 735, 27
Knutson, H. A., Lewis, N., Fortney, J. J., et al. 2012, ApJ, 754, 22
Langton, J., & Laughlin, G. 2008, ApJ, 674, 1106
Laughlin, G., Deming, D., Langton, J., et al. 2009, Nature, 457, 562
Lee, J.-M., Fletcher, L. N., & Irwin, P. G. J. 2012, MNRAS, 420, 170
Lewis, N. K., Showman, A. P., Fortney, J. J., et al. 2010, ApJ, 720, 344
Lewis, N. K., Knutson, H. A., Showman, A. P., et al. 2012, in prep
Lodders, K. 2004, ApJ, 611, 587
Lodders, K. 2010, in Principles and Perspectives in Cosmochemistry, ed. A. Goswami & B. E. Reddy, 379
Lodders, K., & Fegley, B., Jr. 2002, Icarus, 155, 393
Madhusudhan, N., Harrington, J., Stevenson, K. B., et al. 2011, Nature, 469, 64

Madhusudhan, N., & Seager, S. 2009, ApJ, 707, 24
Madhusudhan, N., & Seager, S. 2011, ApJ, 729, 41
Moses, J. I., Visscher, C., Fortney, J. J., et al. 2011, ApJ, 737, 15
Moses, J. I., Madhusudhan, N., Visscher, C., & Freedman, R. S. 2012, ApJ, submitted
Prinn, R. G., & Barshay, S. S. 1977, Science, 198, 1031
Rauscher, E., & Menou, K. 2012, ApJ, 745, 78
Seager, S., & Sasselov, D. D. 2000, ApJ, 537, 916
Shabram, M., Fortney, J. J., Greene, T. P., & Freedman, R. S. 2011, ApJ, 727, 65
Showman, A. P., Cooper, C. S., Fortney, J. J., & Marley, M. S. 2008, ApJ, 682, 559
Showman, A. P., Fortney, J. J., Lian, Y., et al. 2009, ApJ, 699, 564
Smith, M. D. 1998, Icarus, 132, 176
Stevenson, K. B., Harrington, J., Nymeyer, S., et al. 2010, Nature, 464, 1161
Stone, P. H. 1976, in Jupiter, ed. T. Gehrels (Tuscon, AZ: Univ. Arizona Press), 586–618
Swain, M. R., Vasisht, G., & Tinetti, G. 2008, Nature, 452, 329
Swain, M. R., Tinetti, G., Vasisht, G., et al. 2009a, ApJ, 704, 1616
Swain, M. R., Vasisht, G., Tinetti, G., et al. 2009b, ApJ, 690, L114
Swain, M. R., Deroo, P., Griffith, C. A., et al. 2010, Nature, 463, 637
Tinetti, G., Deroo, P., Swain, M. R., et al. 2010a, ApJ, 712, L139
Tinetti, G., Griffith, C. A., Swain, M. R., et al. 2010b, Faraday Discuss., 147, 369
Visscher, C., & Fegley, B., Jr. 2005, ApJ, 623, 1221
Visscher, C., Lodders, K., & Fegley, B., Jr. 2006, ApJ, 648, 1181
Visscher, C., Lodders, K., & Fegley, B, Jr. 2010a, ApJ, 716, 1060
Visscher, C., & Moses, J. I. 2011, ApJ, 738, 72
Visscher, C., Moses, J. I., & Saslow, S. A. 2010b, Icarus, 209, 602
Waldmann, I. P., Tinetti, G., Drossart, P., et al. 2012, ApJ, 744, 35
Wright, J. T., Fakhouri, O., Marcy, G. W., et al. 2011, PASP, 123, 412